TRENDS IN SCIENCES 2026; 23(6): 12035
https://doi.org/10.48048/tis.2026.12035 RESEARCH ARTICLE

Ethanol Extract of *Ocimum Sanctum* Leaves Exerts Apoptotic Activity on A549 Non-Small Lung Adenocarcinoma Cell Line through Down-Regulated of Nf-kb and Activated of Apaf-1

Ulayatul Kustiati[1,2], Dewi Ratih Tirto Sari[3], Golda Rani Saragih[4], Chairunisa Isnainingrum[4], Muhammad Lokman Md Isa[5], Dwi Aris Agung Nugrahaningsih[6], Yudy Tjahjono[7], Dwi Liliek Kusindarta[3], Srikanth Karnati[8] and Hevi Wihadmadyatami[3,*]

[1]*Study Program of Veterinary Science, Faculty of Veterinary Medicine, Universitas Gadjah Mada, Special Region of Yogyakarta 55281, Indonesia*
[2]*Laboratory of Veterinary pharmacology, Faculty of Veterinary Medicine, Universitas Brawijaya, East Java 65151, Indonesia*
[3]*Department of Pharmacy, Faculty of Medical Science, Universitas Ibrahimy, East Java 68374, Indonesia*
[4]*Department of Anatomy and Cell Biology, Faculty of Veterinary Medicine, Universitas Gadjah Mada, Special Region of Yogyakarta 55281, Indonesia*
[5]*Department of Basic Medical Science, Kulliyyah of Nursing, International Islamic University Malaysia, Pahang 53100, Malaysia*
[6]*Department of Pharmacology and Therapy, Faculty of Medicine, Public Health and Nursing, Universitas Gadjah Mada, Special Region of Yogyakarta 55281, Indonesia*
[7]*Biomedical Laboratory, Faculty of Pharmacy, Widya Mandala Catholic University, Surabaya 60265, Indonesia*
[8]*Institute of Anatomy and Cell Biology, Julius-Maximillian's-University Würzburg, Würzburg 907070, Germany*

([*]Corresponding author's e-mail: heviwihadmadyatami@ugm.ac.id)

Received: 24 September 2025, Revised: 21 November 2025, Accepted: 28 November 2025, Published: 20 February 2026

Abstract

Lung cancer was among the primary contributors to mortality within the realm of cancer-related ailments. Multiple research projects had demonstrated *Ocimum sanctum*'s diverse biological and pharmacological characteristics, including its antioxidant, neuroprotective, and anti-cancer capabilities. However, limited evidence supported the assertion that *O. sanctum* on human lung adenocarcinoma cancer cells. Here, we inspected ethanol extract *O. sanctum*'s (EEOS) impact on cellular apoptosis and the suppression of Nuclear Factor kappa-light-chain-enhancer of activated B cells (NF-κB) in A549 human lung adenocarcinoma cancer cells. The chemical composition of EEOS was analyzed using gas chromatography-mass spectrometry (GC-MS), while antioxidant potential was assessed via the DPPH radical scavenging assay. Apoptotic activity was evaluated through Hoechst 33342 nuclear staining, mitochondrial membrane potential (JC-1) assay, and Reactive Oxygen Species (ROS) detection using DCFH-DA. Protein expression of NF-κB, Apoptotic Protease Activating Factor 1 (Apaf-1), caspase-9, and caspase-3 was quantified by ELISA. Molecular docking was performed to explore the interactions between linoleic acid - the predominant compound identified in EEOS - and key apoptotic proteins. Additionally, the *in vivo* chemoprotective effect of EEOS was evaluated in benzo(a)pyrene (B(a)P)-induced lung toxicity in C3H mice. GC-MS profiling identified 33 compounds in EEOS, with linoleic acid, phytol, and β-sitosterol as the major constituents. EEOS exhibited moderate antioxidant activity (IC_{50} = 46.42 µg/mL). Treatment with EEOS significantly induced apoptosis in A549 cells, disrupted mitochondrial membrane potential, and elevated intracellular ROS levels. ELISA analysis showed downregulation of NF-κB and upregulation of Apaf-1, caspase-9, and caspase-3 in a dose-dependent manner. Molecular docking revealed strong binding affinity of linoleic acid to NF-κB and

caspase proteins, comparable to cisplatin. *In vivo*, EEOS mitigated B[a]P-induced lung tissue damage. In conclusion, EEOS exerts potent pro-apoptotic effects through NF-κB inhibition and activation of the intrinsic Apaf-1/caspase-dependent pathway, supporting its potential as a promising adjunct therapy for lung cancer treatment.

Keywords: *Ocimum sanctum*, NF-kB, Apoptotic, Apaf-1, Caspase

Introduction

Lung alveolar pulmonary adenocarcinoma has been a prominent factor in the prevalence of lung cancer and has been linked to considerable mortality rates on a global scale [1,2]. Lung cancer was the most general lead of mortality among cancer patients in Indonesia [3]. The incidence of lung cancer in Indonesia has exhibited a progressive increase over time, and patients experience the disease at a younger age than in other nations [4]. Global Cancer Observatory (GLOBOCAN) data estimate that there were approximately 2.2 million new cases of lung cancer globally in 2020, accounting for roughly 11.4% of all cancer diagnoses. Furthermore, lung cancer mortality is alarming: around 1.8 million deaths were reported in the same year, representing approximately 18% of total cancer-related fatalities [4,5]. The epidemiology of lung cancer reflects significant geographical variations, which largely correlate with patterns of tobacco use. In many high-incidence regions, particularly in countries with high smoking prevalence, such as Indonesia (54.4%) and China (41.5%), the incidence rates of lung cancer are continuing to rise, which poses pressing concerns for public health initiatives [4].

Smoking habits and environmental variables, including air pollution and industrial waste, such as dust, fly ash, bottom ash, and coal ash, are to blame for the higher incidence of lung adenocarcinoma in Indonesia than in other countries [6,7]. Numerous jobs and industries in Indonesia involve various carcinogenic substances. These include asbestos and silica, which are prevalent in construction and restoration activities, and the welding fumes found in steel processing sectors. Additionally, truck drivers and machine engine operators have been exposed to diesel exhaust, posing a carcinogenic risk [7]. As concurrent therapeutic modalities for the treatment of lung cancer, several clinical therapies have shown efficacy, including radiotherapies, chemotherapy, surgery, and allopathic medicine [8]. Nevertheless, unpleasant reactions, such as the development of chemoresistance in tumors, are frequently linked with these therapeutic interventions [9]. Moreover, especially in numerous developing countries, these therapies have imposed a considerable cost burden on healthcare systems [10]. Therefore, there has been significant demand for adjunct and/or alternative medicines.

The assessment of therapeutic plants for the prevention of chemotherapy is crucial, as such plants have the potential to offer efficacious therapeutic alternatives with fewer unwanted effects than conventional allopathic treatment [8]. Emerging studies indicate that using plant-derived or herbal therapeutic interventions might reduce cancer mortality rates by as much as 25%, underpinning the important impact plants or herbal medicine could have in mitigating cancer symptoms and aiding therapy [11,12]. Botanical formulations have been increasingly used as supplementary components in cancer therapy [13]. A polyherbal mixture decoction has long been used as a cancer treatment by Ayurvedic practitioners [14]. Herbal formulations have significantly impacted the regulation of various disease targets through different pathways, such as mitigating adverse effects, improving efficacy, overcoming drug resistance mechanisms, and regulating transporters and enzymes to enhance drug bioavailability [15,16]. The herbal treatments mentioned have shown potential as anti-cancer agents by enhancing the immune system, mitigating chemotherapy toxicity, and improving patients' survival rates [17]. In addition, herbal therapies have been widely employed as supplementary and alternative medicines in several geographical areas, such as the United Kingdom (UK), Europe (France and Germany), North America, and Australia [18]. Moreover, a substantial percentage - specifically, 83% - of chemotherapeutic medicines that have obtained approval from the Food and Drug Administration (FDA) are sourced from natural origins [19].

Ocimum sanctum, a member of the Lamiaceae family, was often distributed in tropical and subtropical

regions, such as Indonesia, India, and Thailand [20]. *Ocimum sanctum L*. (Holy Basil), a revered herb in Ayurvedic medicine, has been utilized for centuries for its diverse therapeutic properties [21]. Modern pharmacological investigations have validated many of these traditional claims, establishing the significance of Holy Basil in contemporary phytomedicine. This validation is largely attributed to its rich phytochemical profile, which includes essential oils, flavonoids, and triterpenoids [22,23]. Several studies have provided evidence for *O. sanctum*'s various biological and pharmacological properties, such as its anti-inflammatory, antioxidant, antibacterial, neuroprotective, and anti-cancer activities [24-27]. The potential anti-cancer effects of the extract obtained from the leaves of *O. sanctum* have been extensively studied in different tumor types, such as gastric [28], pancreatic [29], colorectal [30], lung [31], and head and neck cancers [20,32].

A major focus in cancer research is the modulation of key survival and death pathways [9]. Notably, *O. sanctum* and its extracts have been extensively shown to exert anti-inflammatory effects, primarily through the downregulation of the nuclear factor kappa-light-chain-enhancer of activated B cells (NF-κB) signaling pathway [30]. Since the NF-κB transcription factor is frequently constitutively activated in cancer - including non-small cell lung cancer (NSCLC) - its inhibition is a critical step in suppressing tumor growth and sensitizing cells to apoptosis [33]. Furthermore, the compounds in Holy Basil are known to directly influence the intrinsic apoptotic cascade, often by promoting the expression and activation of pro-apoptotic factors such as apoptotic protease activating factor 1 (Apaf-1), which is central to the formation of the apoptosome [34]. However, a comprehensive explanation of the specific cellular mechanisms behind the anti-cancer properties of Ethanol extract *O. sanctum*'s (EEOS) leaves is lacking. Given these findings, we hypothesize that **EEOS** may exert cytotoxic and apoptotic effects on A549 NSCLC cells through the modulation of these pathways. The present study investigates the potential of *O. sanctum* ethanol extract to induce apoptosis via the **downregulation of NF-κB** and **activation of Apaf-1**, providing mechanistic insight into its anticancer properties.

Materials and methods

Plant extract preparation

Sourced of *O. sanctum* Linn dried leaves from CV Merapi Farma Herbal, Industries engaged in traditional medicine and medicinal plant cultivation in Special Region of Yogyakarta, Indonesia. Extract preparation was carried out by maceration technique, method was taken from Kustiati *et al.* [35]. *O.sanctum* Linn grinded dried leaves weighed as much as 300 g and mixed with 96% ethanol as much as 4,000 mL. The mixture was filtered twice to produce a filtrate. To get a thick extract, the filtrate was evaporated in a waterbath at 60 °C using a vacuum rotary evaporator. The filtrate will be evaporated until it becomes a paste with a yield of around 9%.

Chemical compound characterization using GC-MS

Gas Chromatography-Mass Spectrometer study was executed with Gas chromatography (Thermo ScientificT^{M} series TRACE 1310) and Mass Spectrometer (Thermo Scientific^{TM} series ISQ LT Single Quadrupole). This method referred to Putri *et al*. [36] with some adjustment. The sample was dissolved in ethanol absolute, homogenized, and centrifuged at 9,500 rpm for 3 min. A 1 µL of sample was injected to the GC-MS. The GC-MS equipment in condition in a provider gas of ultra-high pure (UHP) helium, an injector at 290 °C, 10 mL/min mobile phase flow rate, 10 split ratio, 1 mL/min front inlet flow, an MS switch line at 230 °C, an ion supply at 200 °C, 3 mL/min purge flow, 5 mL/min gas saver flow, and a gas saver time at 5 min. The study was conducted at a relative humidity of 55% and room temperature of 23 °C. An HP-5MS UI column with a length of 30 m, an inner diameter of 0.25 mm, and a film thickness of 0.25 µm was used to store the GC-MS statistics. The NIST 14 standard library was used to establish the compound's molar mass.

In silico molecular docking

Ligand structure retrieval and modeling

The PubChem database provided the 3D structure of linoleic acid (CID 5280450). Using the Corina software, the structure of cisplatin (CID 5702198) was modeled. (https://demos.mn-am.com/corina.html). Canonical smiles of cisplatin from PubChem were

copied and pasted into the Corina program, and then the structure in pdb format was downloaded.

Protein 3D structure retrieval and preparation

The Protein Data Bank was used to retrieve the target protein's 3D structure. The target and access code of each protein includes Nf-κB (PDB ID 1NFI), Apaf-1 (PDB ID 4RHW), Caspase 3 (PDB ID 3DEJ), Caspase 9 (PDB ID 4RHW). Molegro virtual docker version 5.0 was used to load the protein structures. The preparation was done by removing the solvent and ligand attached, then predicting the active side of each protein with a maximum molecular surface van der Waals expansion parameter of 5. The active side is displayed in the protein grid that will be used for docking.

Molecular docking simulation

Target protein and target ligand were interacted using Molegro virtual docker version 5.0 (Bitencourt-Ferreira & De Azevedo, 2019). Docking was performed on specific regions of each protein grid. The Nf-κB protein grid is X = −5.28; Y = 54.24; Z = −16.46 Radius 8, Apaf-1 protein grid X = −14.17, Y = −26.38; Z = 5.91; Radius 13, Caspase 3 protein grid X = -50.50; y = 5.37; z = −55.24, Radius 7, and Caspase 9 protein grid x = −15.61; y = −20.54; z = 0.44; Radius 10.

Antioxidant activity using DPPH assay

The DPPH technique was carried out in accordance with the earlier approach described by Sukweenadhi *et al.* [37] with a few minor adjustments. Solution of 2,2-diphenyl-2-picrylhydrazyl (DPPH) (Sigma-Aldrich, Missouri, USA) was prepared by weighing 1.98 mg DPPH powder in ethanol absolute with volume 20 mL and then incubating it in the dark for 2 h. As a positive control of antioxidant activity, L-Ascorbic acid was prepared by adding L-Ascorbic acid was diluted in ethanol absolute and prepared into gradient solution starting at 10 with 10 µg/mL increments at each concentration until 100 µg/mL. Ethanolic Extract *O. sanctum* Linn as sample was dissolved in absolute ethanol absolute with a definite concentration of 100 µg/mL and diluted with the same concentration gradient as L-ascorbic acid. DPPH solution was moved to a conical tube and then added with EEOS according to concentration and Tris-HCl Buffer 0,1 M, pH 7,4 (Sigma-Aldrich, Missouri, USA) pH 7.4 in a ratio of 5:1:4 (DPPH solution: Sample/standard: Tris-HCL Buffer), homogenized - blank solution as standard solution by adding DPPH solution with Tris-HCl buffer with ration 6:4. Blank solutions and various concentrations of L-Ascorbic Acid and EEOS were allowed to stand for 30 min, transferred to 96-well plates, and triplicated. Absorbance values were read using a multimode microplate reader (Spark Tecan, Tecan Trading AG, Switzerland) at 517 nm wavelength. The absorbance data acquired were calculated using the inhibition percentage formula to get the inhibition proportion. The absorbance value of each sample and blank was calculated using percentage inhibition formula:

$$Scavenging\ effect\ (\%) = \frac{Standard\ absorbance - Sample\ absorbance}{Standards\ absorbance} \times 100\%$$

Cultivation of A549 human lung adenocarcinoma

The A-549 cells were cultivated in a T25/T75 flask using DMEM high glucose media supplemented with 10% FBS (Capricorn, Ebsdorfergrund, Jerman), 0.5% penicillin-streptomycin (Capricorn, Ebsdorfergrund, Jerman), and 0.5% amphotericin B (Capricorn, Ebsdorfergrund, Jerman). The cells were then incubated at 37 °C with 5% CO_2. The media was changed at 3-day intervals and subcultured when reaching a confluence state. The cells were collected using an accurate cell detachment solution containing 0.5 mM EDTA.4Na (Capricorn, Ebsdorfergrund, Jerman) and subsequently used for the experiment.

Hoechst staining 33242

A coverslip was positioned at the bottom of each 24-well plate containing A549 cells. Approximately 80% confluence was attained by the cells after they were incubated. The cells were treated with complete medium for the untreated group, 80 µg/mL of AP3 as a positive control, 9 µg/mL of cisplatin, and EEOS at progressively lower concentrations (200, 100, 70 and 50 µg/mL) after confluence was reached. The medium was taken out after a day, and sterile DPBS was used to rinse the wells. To fix the cell, 70% ethanol was used in cold conditions. The fixative solution was then disposed of, and DPBS was used to rinse the cells once again. Each well was then filled in the dark with 250 µL of 1 µg/mL Hoechst 33342 dye (ThermoFisher Scientific,

Massachusetts, USA). After 10 min of room temperature incubation, the cells were examined under a confocal microscope (Zeiss Oberkochen, Germany). By comparing living cells and dead cells, the cell death rate can be calculated. Living cells have a normal nucleus morphology, but dead cells have a shrunken nucleus in contrast. With 3 observers, calculations were performed in 5 fields of vision. After that, the number of cells was determined using the formula below:

$$\text{Apoptosis rate} = \frac{\text{death cell}}{\text{live cell}} \times 100\%$$

JC-1 staining for mitochondrial membrane potential assay

A549 cells were cultured on well plates with the adjusted amount and incubated until confluent. After reaching 80% confluence, cells were treated in 7 groups: Negative control group with complete media, positive control with 80 µg/mL AP3, 9 µg/mL cisplatin, and EEOS with various concentrations (200, 100, 70 and 50 µg/mL). The treatment was carried out for 24 h. The media was removed and rinsed with JC-1 buffer solution, JC-1 Working solution 2 µg/mL was added and incubated again for 20 min, the dye was removed and rinsed with JC-1 buffer solution twice, the cells were observed on a flowcytometry with excitation of 585 nm and emission of 590 nm.

Reactive Oxygen Species (ROS) assay using DCFH-DA

Cells were grown in well plates until confluent, after confluent cells were given treatment and incubated for 24 h, the cells were detached after treatment and centrifuged to separate cells and detachment solution. DCFH-DA probe 10µM in medium free serum was poured into the well, each treatment got the same volume and incubated for 30 min in dark conditions. After incubation, centrifugation was carried out to remove the probe and washed once before being observed using a BD FACSAriatm III flowcytometry (Becton Dickinson Bioscience, New Jersey, USA) with a wavelength of 488 and 525 nm for excitation and emission.

A549 lysate preparation

The 5×10^5 A-549 cells/mL were cultured in individual wells of a 6-well tissue culture plate and then incubated for 1 h. The treatments in each are i) non-treated (NT); ii) AP3 80 µg/mL; iii) cisplatin 9 µg/mL; iv) EEOS 50 µg/mL; v) EEOS 70 µg/mL; vi) EEOS 100 µg/mL; vii) EEOS 150 µg/mL; viii) EEOS 200 µg/mL. The cells were incubated for 24 h. The media was aspirated and washed on the plate using Dulbecco's phosphate-buffered saline (DPBS) (Capricorn, Ebsdorfergrund, Jerman). Subsequently, 700 µL of ready-to-use radioimmunoprecipitation assay (RIPA) lysis buffer (*Thermofisher Scientific,* AS) buffer was added. The plate underwent agitation for 15 min. Cells were extracted from the bottom of the plate using a cell scraper. The lysate was aliquoted into 1.5 mL microtubes and centrifugated at 6,500 rpm for 10 min at 4 °C. Subsequently, the supernatant was conscientiously moved to another 1.5 mL microtubes.

Protein expression using Enzyme-Linked Immunosorbent Assay (ELISA)

This assay utilized human APAF-1, Capase3, caspase 9 (Fine Test, Wuhan, China), and NF-κB (Abclonal, Massachusetts, USA) ELISA KIT. The steps were followed in accordance with the instructions in the kit (Fine Test, Wuhan, China; Abclonal, Massachusetts, USA). Prior to adding lysate and standard samples, the plate was washed twice. Each well received 100 µL of the standard and sample, which were then incubated at 37 °C for 90 min. Two washes and aspiration were performed on the plate. After adding 100 µL of Biotin-labeled antibody, the mixture was incubated at 37 °C for 60 min. Wash the plate 3 times after aspirating it. Each well received 100 µL of HRP-Strepvidin Conjugate (SABC) working solution, which was then incubated at 37 °C for 30 min. The plate underwent 5 rinses and aspirations. The 90 µL TMB substrate was added, and it was incubated at 37 °C for 15 to 30 min. Fifty µL of stop solution was added, and the well plate was immediately read at 450 nm.

Study of the acute effects of a single high dose of benzo(a)pyrene in C3H mice

Approval No. 00053/EC-FKH/Int./2021 from the Gadjah Mada University Faculty of Veterinary Medicine is the ethics committee's approval number for

this project. In this investigation, male C3H mice (Charles River, Strain code 025) between the ages of 6 and 8 weeks were employed with weighing approximately 19 - 22 g. Polycarbonate cages (Techniplast, Buguggiate, Italy) were utilized to house the mice. The mice were kept in controlled environments with a controlled light-dark cycle, a temperature of 22 - 24 °C, and a humidity of 55% - 65%. They were also given unlimited access to food and drink. Four groups of 5 mice each were randomly selected from among the animals. Specifically, the following groups were used: (a) a negative control group using corn oil as the vehicle; (b) a positive group receiving a single dose of Benzo(a)pyrene (B(a)P) (125 mg/kg in corn oil) orally in day-7; (c) EEOS (150 mg/kg) only given orally from day-1 to day-7 (d) EEOS (150 mg/kg) given orally from day-1 to day-7, followed by a single dose of B(a)P (125 mg/kg in corn oil). On day-7, 2 h following the delivery of EEOS, a high single dosage of B(a)P was given. The mice were killed the next day so that blood samples could be taken in Ethylenediaminetetraacetic acid (EDTA) and lung samples could be taken for further examination.

Data analysis

Docking data was analyzed and visualized with PyMol 2.3 and Discovery Studio version 21.1.1. Data analysis was in the form of a 3D and 2D structure display, the interaction between ligand and protein, and binding energy. DPPH Assay and ELISA result was analyzed IC50 and One-way ANOVA using GraphPad Prism ver 8.

Results and discussion

Chemical composition of the ethanolic extract of *O. sanctum* Linn leaves

The chemical components and secondary metabolites of the extracted EEOS were analyzed with gas chromatography-mass spectrometry (GC-MS). This method involved detecting the volatile substances produced by the sample. Although the GC-MS spectra found numerous secondary metabolite chemicals in each sample, this analysis exclusively incorporates matching values exceeding 90% into the NIST MS library. Approximately 33 substances, predominantly sesquiterpenes, fatty acids, esters, and steroids, have been found. The chemical structures of the detected chemical compounds with a matching value exceeding 90% are presented in **Table 1** and **Figure 1**.

Multiple retention times observed for certain compounds (e.g., 7-epi-trans-Sesquisabinene hydrate, melezitose, and 1-Heptatriacotanol) may indicate the presence of isomeric forms or structural analogues of these metabolites. Such isomerism has been reported in previous GC-MS studies of *O. sanctum* essential oils and ethanolic extracts, where temperature sensitivity and compound volatility often cause co-elution or separate minor peaks for closely related molecular structures [38,39]. This phenomenon is a direct consequence of the presence of stereoisomers. Stereoisomers are compounds that have the same chemical formula and sequence of bonded atoms but differ in the 3-dimensional orientations of their atoms in space [40]. For sesquiterpenes such as 7-epi-trans-Sesquisabinene hydrate, the multiple retention times indicate the separation of geometric isomers (e.g., *cis/trans* configurations) and/or epimers (stereoisomers differing at only one chiral center) [41]. Similarly, the multiple peaks for 3-Hydroxydodecanoic acid are due to the presence of both the (R)- and (S)-enantiomers [42]. Although these molecules have identical mass spectra, the chiral stationary phase of the GC column separates these stereoisomers, leading to distinct peaks on the chromatogram. For the purposes of reporting, the best-matched compound name from the NIST library is used to represent the group of co-eluting isomers.

Table 1 Chemical composition of ethanolic extract of *O. sanctum* Linn leaves.

Retention time (min)	Molecular name	Molecular formula	Molecular weight	Relative area (%)
11.17	Linalool	$C_{10}H_{18}O$	154	0.61
15.28	Geranic acid	$C_{10}H_{16}O_2$	168	2.79
15.47; 17.62; 18.81	7-epi-trans-Sesquisabinene hydrate	$C_{15}H_{26}O$	222	0.29; 1.30; 0.87

Retention time (min)	Molecular name	Molecular formula	Molecular weight	Relative area (%)
15.77; 16.70; 18.60; 20.89	3-Hydroxydodecanoic	$C_{12}H_{24}O_3$	216	0.14; 0.56; 0.46; 0.36
16.08	Caryophyllene	$C_{15}H_{24}$	204	0.90
16.23	cis-a-Bergamotene	$C_{15}H_{24}$	204	0.59
16.53	Humulene	$C_{15}H_{24}$	204	0.37
16.64; 18.08; 20.75; 22.75; 25.93; 29.39	1-Heptatriacotanol	$C_{37}H_{76}O$	536	0.14; 0.13; 0.26; 0.12; 0.69; 0.48
16.81	Inosine	$C_{10}H_{12}N_4O_5$	268	1.54
16.88	Nerolidol acetate	$C_{17}H_{28}O_2$	264	2.57
16.99; 19.17; 19.34	Desulphosinigrin	$C_{10}H_{17}NO_6S$	279	2.12; 1.16; 0.73
17.06; 17.15; 17.28; 17.42; 21.92	Melezitose	$C_{18}H_{32}O_{16}$	504	3.86; 1.92; 0.71; 0.61; 0.15
17.56	cis-a-Bisabolene	$C_{15}H_{24}$	204	2.77
18.16; 18.47	Caryophyllene oxide	$C_{15}H_{24}O$	220	1.08; 0.48
18.91	Pterin-6-carboxylic acid	$C_7H_5N_5O_3$	207	0.44
18.99; 19.10	Tetraacetyl-d-xylonic nitrile	$C_{14}H_{17}NO_9$	343	1.47; 1.05
20.82	Neophytadiene	$C_{20}H_{38}$	278	1.97
20.95; 22.90; 22.98	9-Hexadecenoic acid	$C_{16}H_{30}O_2$	254	0.25; 0.24; 0.57
21.26	3,7,11,15-Tetramethyl-2-hexadecen-1-ol	$C_{20}H_{40}O$	296	0.91
21.69	Hexadecanoic acid, methyl ester	$C_{17}H_{34}O_2$	270	0.41
22.11	n-Hexadecanoic acid	$C_{16}H_{32}O_2$	256	7.73
23.08; 26.74; 28.17; 28.35; 30.46; 33.78	Ethyl iso-allocholate	$C_{26}H_{44}O_5$	436	0.26; 0.22; 0.18; 0.39; 0.18; 0.18
23.33	9,12-Octadecadienoic acid, methyl ester, (E,E)-	$C_{19}H_{34}O_2$	294	0.13
23.39	9,12,15-Octadecatrienoic acid, methyl ester, (Z,Z,Z)	$C_{19}H_{32}O_2$	292	0.93
23.51	Phytol	$C_{20}H_{40}O$	296	5.48
23.72	Linoleic acid	$C_{18}H_{32}O_2$	280	15.94; 1.22
23.83; 23.91	Linolenic acid	$C_{18}H_{30}O_2$	278	1.90
23.97	Octadecanoic acid	$C_{18}H_{36}O_2$	284	1.37
26.04	6,9,12-Octadecatrienoic acid, methyl ester	$C_{19}H_{32}O_2$	292	0.41
33.25	dl-a-Tocopherol	$C_{29}H_{50}O_2$	430	0.55
35.02	Campesterol	$C_{28}H_{48}O$	400	0.77
35.63	Stigmasterol	$C_{29}H_{48}O$	412	0.78
36.86	ß-Sitosterol	$C_{29}H_{50}O$	414	3.32

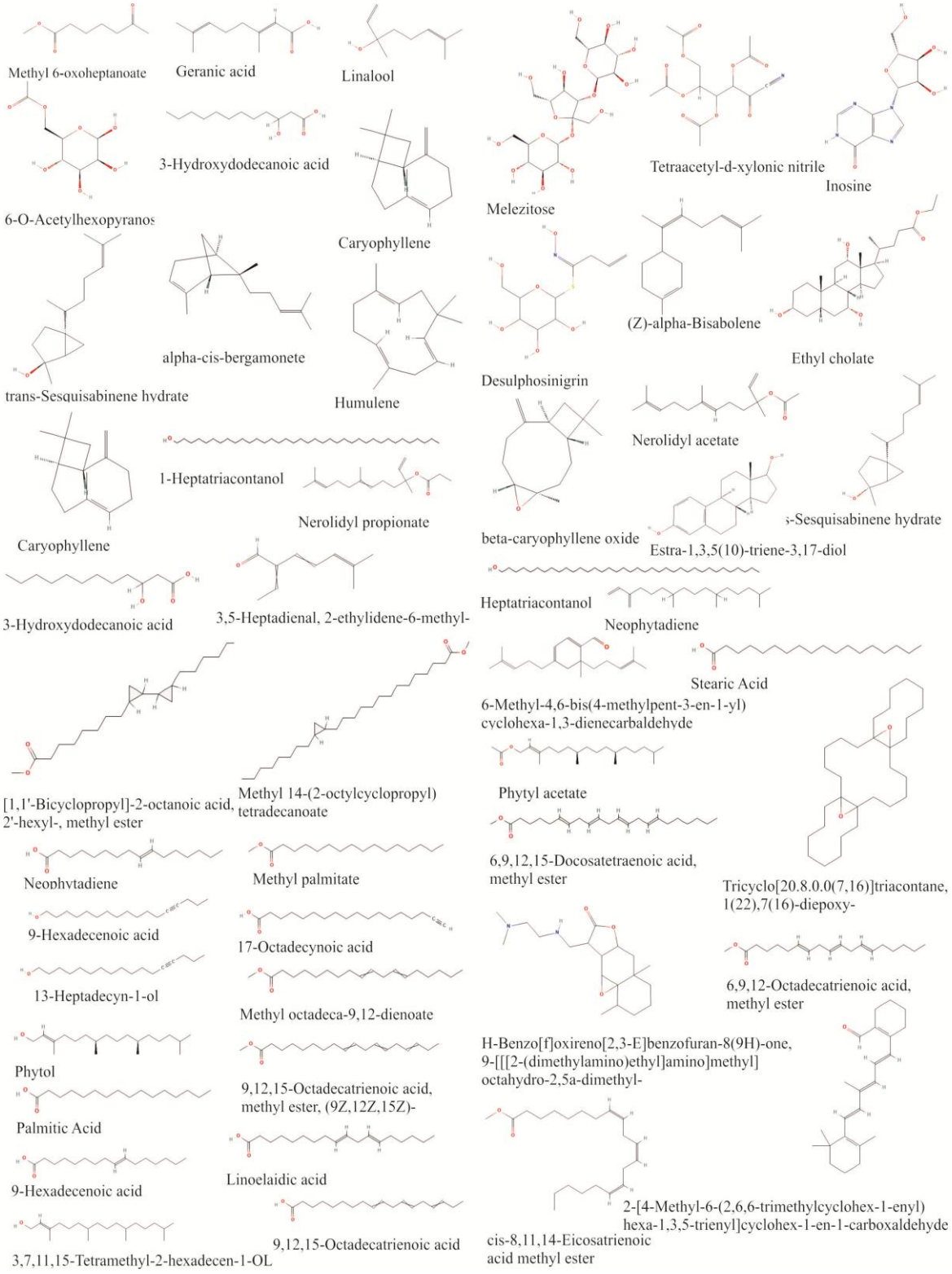

Figure 1 Chemical Compounds Structure of EEOS analyzed by GC-MS.

According to GC-MS untargeted screening findings of EEOS active chemicals, linoleic acid is the biggest of 33 metabolite compounds found in EEOS.

The overall GC-MS profile of the EEOS in this study aligns well with earlier reports of *O. sanctum* phytochemistry, which identified linoleic acid, phytol, caryophyllene, eugenol, and β-sitosterol as major constituents [23,43,44]. These bioactive compounds are associated with the plant's antioxidant, anti-inflammatory, and anticancer properties, supporting the

biological relevance of our extract composition. Specifically, the identification of compounds such as linalool and caryophyllene is consistent with previous studies on *O. sanctum* extracts, which frequently cite these as key active constituents alongside major compounds such as eugenol and ursolic acid. The presence of a high relative area of terpenoids (including sesquiterpenes) and fatty acids in our ethanol extract is particularly noteworthy [45,46]. For instance, while monoterpenoids like eugenol are characteristic, the significant detection of sesquiterpenes (e.g., 7-epi-trans-Sesquisabinene hydrate) and hydroxy fatty acids (e.g., 3-Hydroxydodecanoic acid) underscores the depth of chemical complexity of the EEOS, which may vary due to geographic origin, harvest time, and extraction method. The presence of these specific classes is chemically relevant, as many sesquiterpenes and medium-chain hydroxy fatty acids have been previously linked to anticancer [47] and anti-inflammatory activities [48]. This chemical fingerprint, particularly the synergistic presence of these components, provides the mechanistic foundation for the observed apoptotic activity of the EEOS against the A549 cell line.

Linoleic acid inhibits the active side of Nf-Kb, Apaf-1, Caspase-9, and Caspase-3

Linoleic acid inhibits Nf-κB activity by binding to IκB (inhibitor of κB), while cisplatin binds to both IκB and Nf-κB. IκB residues bound by linoleic acid are LEU223, ILE192, LEU189, ASN145, ASN182, and HIS184 (Figure 2A and Table 2). Cisplatin binds to IκB residues at ASP226 and Nf-κB residues (ASP210, GLY208, and ARG253). Linoleic acid binds between Apaf-1 and Caspase-9. Apaf-1 residues bound by linoleic acid are ARG44, ARG52, THR22, and SER23, while caspase-9 residues bound by linoleic acid are ALA46 (Figure 2B and Table 2). Cisplatin binds to Caspase-9 residues at ARG6, ARG10, ASP61, and MET39. The Apaf-1 residues to which cisplatin binds are TYR24, GLN49, GLN50, GLU41, and THR48. The binding of these residues causes the activation of Caspase-9 by Apaf-1.

Linoleic acid and cisplatin bind to Caspase-9 at the Caspase-9 activator region. The residues bound by linoleic acid are ASP42, ARG45, ALA46, and ILE43 (**Figure 2(C)** and **Table 2**). Residues ASP42 and ARG45 are also on the active side of cisplatin and caspase-9, indicating that linoleic acid has the same Caspase-9 activation mechanism as cisplatin. Linoleic acid binds to Caspase-3 with 4 hydrogen-bonded residues and 7 hydrophobic interactions. The hydrogen-bonded residues are ARG64, GLN161, ARG207, and SER120. MET61, HIS121, PHE128, and TYR204 were identified to bind with hydrophobic interactions (**Figure 2(D)** and **Table 2**). Cisplatin binds with 2 electrostatic bonds (ARG64 and ARG207) and 2 hydrogen bonds to residue GLU123. Residues ARG64 and ARG207 were also identified on the active side residues of linoleic acid. In addition, some residues bound by linoleic acid are side activators to activate Caspase-3 in the apoptotic mechanism. Based on the binding energy, linoleic acid produces a lower binding energy than cisplatin, which is −320.8 kJ/mol.

Linoleic acid exhibited stronger binding affinities than cisplatin toward all the target proteins, with binding energies ranging from –245.6 to –320.8 kJ/mol, while cisplatin showed energies between –40.0 and –182.6 kJ/mol. These lower (more negative) values indicate higher predicted binding stability and suggest that linoleic acid could effectively interact with and modulate these apoptosis-related proteins [49]. The docking interactions revealed that linoleic acid forms multiple hydrogen bonds and hydrophobic contacts with critical amino acid residues within the active or regulatory sites of the proteins, including ASN182 and HIS184 (NF-κB), ARG52 and THR22 (Apaf-1), ASP42 and ARG45 (Caspase-9), and ARG64 and GLN161 (Caspase-3). Such interactions are essential for the stabilization of protein–ligand complexes and may facilitate activation of the intrinsic apoptotic pathway. These findings are consistent with the in vitro results demonstrating that EEOS downregulated NF-κB expression and upregulated Apaf-1, Caspase-9, and Caspase-3 activity in A549 cells, suggesting that linoleic acid contributes to apoptosis induction via mitochondrial signaling [50,51]. The stronger predicted interaction of linoleic acid compared to cisplatin highlights its potential as a natural modulator of apoptotic signaling, although further biochemical validation is required to confirm this mechanism.

Table 2 Binding energy, Interaction, Distance, and Binding type of ligand (Linoleic acid, most abundant substance in EEOS and cisplatin) and protein target (Nf-κB, Apaf-1, caspase 9, and caspase 3).

Ligand	Protein	Binding Energy (kJ/mol)	Interaction	Distance	Binding type
Linoleic Acid	Nf-κB	−245.6	:10:H32 - F:ASN182:OD1	2.16212	Hydrogen Bond
			F:ASN145:ND2 - :10:O2	2.54885	
			:10 - F:LEU189	4.95058	Hydrophobic
			:10 - F:ILE192	4.4905	
			:10:C12 - F:ILE192	4.55822	
			:10:C12 - F:LEU223	4.17798	
			F:HIS184 - :10	4.67528	
	Apaf-1	−268.2	B:ARG52:NE - :10:O2	2.85334	Hydrogen Bond
			B:ARG52:NH1 - :10:O2	2.9928	
			:10:H32 - B:THR22:OG1	2.77354	
			B:ARG44 - :10	4.22386	Hydrophobic
			B:ARG44 - :10	4.73831	
			B:ARG44 - :10	4.8299	
			E:ALA46 - :10	4.89428	
			E:ALA46 - :10	4.6337	
			B:THR22:N - :10:H32	2.16885	Unfavorable
			B:SER23:N - :10:H32	1.86159	
	Caspase 9	−268.8	:10:H32 - F:ASP42:O	1.71342	Hydrogen Bond
			E:ARG45 - :10	4.61842	Hydrophobic
			E:ALA46 - :10	4.11221	
			F:ARG45 - :10	4.34729	
			:10:C12 - E:ILE43	4.30766	
	Caspase 3	−320.8	D:ARG64:NH2 - :10:O2	2.90959	Hydrogen Bond
			D:GLN161:NE2 - :10:O2	2.92503	
			D:ARG207:NH1 - :10:O1	2.98964	
			:10:H32 - D:SER120:O	2.04719	Hydrophobic
			:10 - D:MET61	5.01617	
			D:HIS121 - :10	4.07815	
			D:PHE128 - :10:C12	4.62644	
			D:TYR204 - :10	4.33219	
			D:TYR204 - :10	5.09966	
			D:TYR204 - :10	4.67347	
			D:TYR204 - :10	5.42909	
Cisplatin	Nf-κB	−90.4	A:ARG253:NH1 - :10:Cl1	5.18849	Electrostatic
			A:ARG253:NH1 - :10:Cl2	5.25359	
			:10:H1 - A:GLY208:O	1.94113	Hydrogen Bond
			:10:H1 - A:ASP210:OD1	2.06189	

Ligand	Protein	Binding Energy (kJ/mol)	Interaction	Distance	Binding type
			:10:H3 - A:GLY208:O	2.04954	
			:10:Pt1 - F:ASP226:OD2	3.57653	
	Apaf-1	−182.6	E:ARG6:NH1 - :10:Cl1	4.65667	Electrostatic
			E:ARG10:NH1 - :10:Cl1	4.79839	
			:10:H1 - E:ASP61:OD2	2.16693	Hydrogen Bond
			:10:H3 - E:MET39:O	2.0765	
			:10:H1 - A:TYR24:OH	2.4747	
			:10:H1 - E:ASP61:OD2	2.73055	
			:10:H2 - E:ASP61:OD2	2.74142	
			:10:H3 - A:TYR24:OH	2.2521	
			:10:H3 - E:MET39:O	2.37061	
			:10:Pt1 - A:GLN49:OE1	3.30203	
			:10:Pt1 - A:GLN50:OE1	3.28255	
			A:THR48:CB - :10:Cl2	3.44529	
			B:GLU41:OE1 - :10:Cl2	3.38415	Unfavorable
	Caspase 9	−49.2	E:ARG45:NH2 - :10:Cl2	3.91686	Electrostatic
			F:ARG45:NH2 - :10:Cl1	3.92005	
			:10:H1 - F:HIS38:NE2	2.70151	Hydrogen Bond
			:10:H1 - F:ASP42:OD1	2.3583	
			:10:H2 - E:ASP42:OD1	1.72156	
			:10:H3 - E:HIS38:NE2	1.97873	
			:10:H3 - F:HIS38:NE2	2.53679	
			:10:H1 - E:HIS38:NE2	2.43547	
			:10:H1 - F:ASP42:OD2	2.47093	
			:10:H2 - E:ASP42:OD2	2.87185	
			:10:H2 - F:HIS38:NE2	2.36696	
			:10:H3 - E:ASP42:OD1	1.72725	
			E:ARG45:NH2 - :10:H2	2.51527	Unfavorable
			E:ARG45:NH2 - :10:H3	2.54375	
	Caspase 3	−40	D:ARG64:NH2 - :10:Cl1	4.28428	Electrostatic
			D:ARG207:NH1 - :10:Cl1	3.437	
			:10:H1 - D:GLU123:OE2	1.69064	Hydrogen Bond
			:10:H3 - D:GLU123:OE2	2.33818	

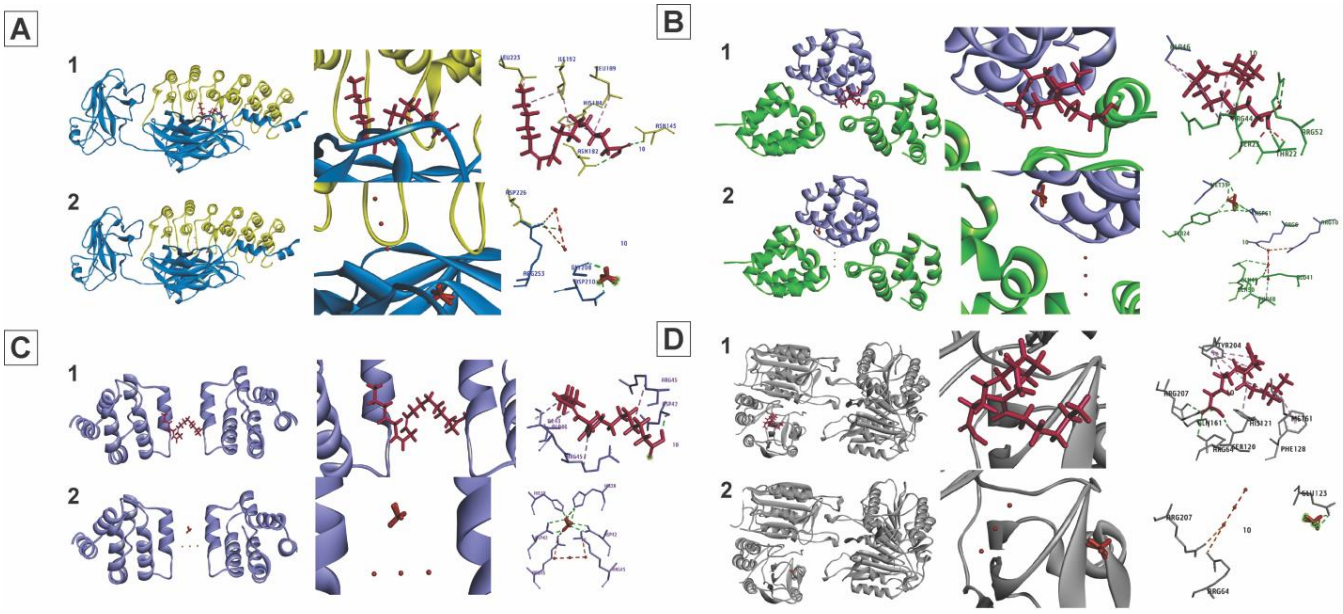

Figure 2 3D and 2D interaction of linoleic acid and cisplatin over targeted protein Nf-κB, Apaf-1, Caspase-9, and Caspase-3. (A) Linoleic acid and cisplatin's interaction with the Nf-κB protein. (1) IκB (yellow) binds to linoleic acid (red), which then attaches to the active side of Nf-κB (blue). (2) The active side of Nf-κB (blue) and IκB (yellow) is bound by cisplatin (red). (B) Interaction of cisplatin and linoleic acid on the APAF-1 protein. (1) Between Apaf-1 (green) and Caspase-9 (purple), linoleic acid (red) binds to the active side. (2) Between Apaf-1 (green) and Caspase-9 (purple), cisplatin (red) attaches itself to the active side. (C) Interaction of cisplatin and linoleic acid on the Caspase-9 protein. (1) The active side of Caspase-9 (purple) is bound by linoleic acid (red). (2) The active side of Caspase-9 (purple) is bound by cisplatin (red). D. Interaction of cisplatin and linoleic acid with the Caspase-3 protein. (1) Between Caspase-3 (gray) and Caspase-9 (purple), linoleic acid (red) binds to the active side. (2) The active side of Caspase-3 (gray) is bound by cisplatin (red).

EEOS antioxidant activity

The DPPH assay was conducted to ascertain the presence of antioxidant chemicals within EEOS that can bind with free radicals. A set of EEOS as samples and L-Ascorbic acid as standard with varying concentrations were subjected to a reaction with DPPH reagent, and the resulting absorbance values were recorded. The acquired absorbance value was converted into a percentage of inhibition, as depicted in **Figure 3**. The IC50 parameter was employed to quantify the antioxidant activity of L-Ascorbic acid and EEOS, specifically referring to the concentration of antioxidants present in EEOS that is necessary to inhibit 50% of the activity of free radicals. The free radical utilized in this experiment is the DPPH reagent, also known as 2,2-diphenyl-1-picrylhydrazyl. The IC50 value derived from L-Ascorbic acid is 30.21 ± 5.02 µg/mL, while the IC50 value of EEOS was higher, at 46.42 ± 3.67 µg/mL.

The observed effect of antioxidants on DPPH is attributed to their ability to donate hydrogen. The results obtained from the DPPH experiment suggest that the EEOS contains molecules that demonstrate the capacity to scavenge free radicals utilizing hydrogen donation [52]. The results showed that EEOS exhibited strong antioxidant activity with an IC50 of 46.42 µg/mL. Antioxidant activity proposed a classification system for evaluating the antioxidant activity of compounds concerning their ability to neutralize free radicals. According to this system, a compound is categorized as possessing an effective antioxidant activity if its IC50 rate is less than 10 µg/mL. Conversely, a compound is classified as having a strong antioxidant activity if its IC50 value is 10 - 50 µg/mL. If the IC50 rate is 50 - 100 µg/mL, the compound is deemed to have a moderate antioxidant activity. On the other hand, a compound is considered to have weak antioxidant activity if its IC50 value ranges from 100 to 250 µg/mL. Finally, a compound is classified as inactive if its IC50 value

exceeds 250 µg/mL. Based on this classification, it can be concluded that the compound under investigation, EEOS, exhibits a strong antioxidant activity in countering free radicals (46.42 ± 3.67) µg/mL) [53].

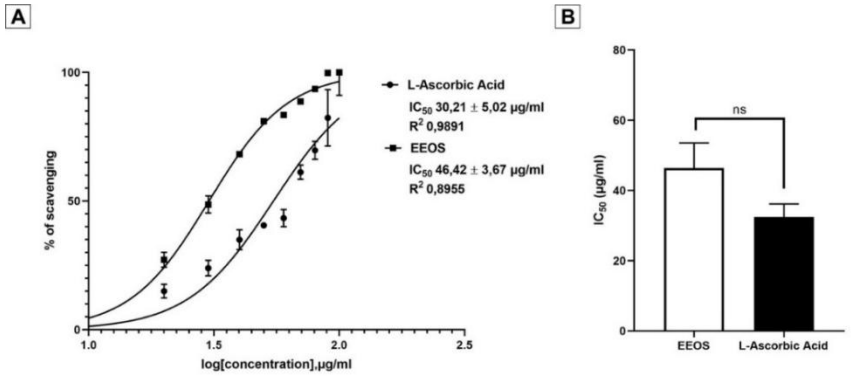

Figure 3 Percentage of EEOS inhibition after DPPH test. (A) DPPH radical scavenging activity of EEOS and L-Ascorbic acid. (B) IC_{50} of EEOS, the IC50 value obtained from L-Ascorbic acid is 30.21 ± 5.02 µg/mL, EEOS 46.42 ± 3.67 µg/mL, and the significant value is non-significant (ns).

EEOS induces apoptosis in A549 cells

The shape change of A549 cells was examined by Hoechst 33342 staining to determine how EEOS caused apoptosis in the cells. Compared to untreated cells, the treated group had a few general apoptotic alterations, including chromosomal aggregation, crenation, apoptotic bodies, and chromatin morphological fragmentation (**Figure 4(A)**). The percentage of apoptosis was calculated by comparing living and dead cells. EEOS was able to significantly increase the rate of apoptosis compared to the control, as indicated by the number of dead cells and the number of cells on observation ($p < 0.001$) (**Figure 4(B)**).

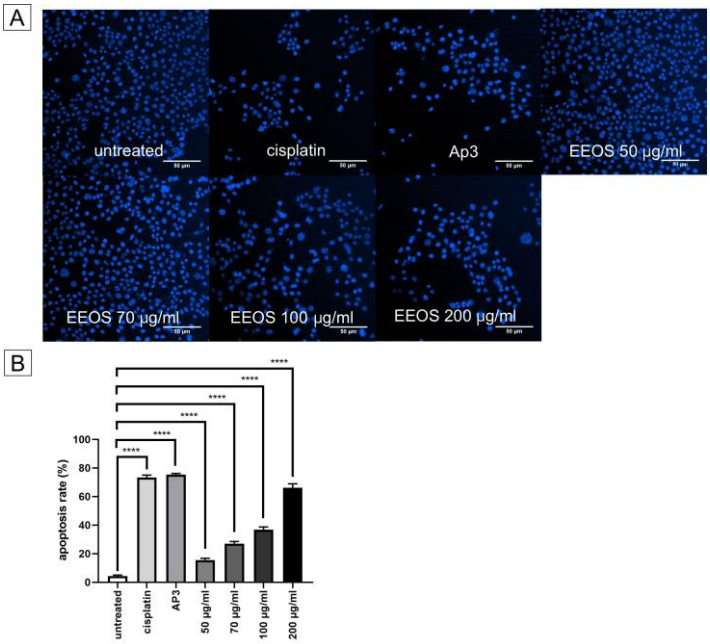

Figure 4 Cellular nuclei of A549 after treatment. (A) The cellular nuclei of A549 cells were stained by Hoechst 33324 staining; the shrinking nuclei of A549 treated by EEOS were observed. (B) Hoechst staining data were performed with 3 repetitions. The statistical analysis of apoptosis rate using a 1-way ANOVA, followed by Tukey's post hoc test, concluded that EEOS can increase the apoptosis rate of an A549 cell line significantly ($p < 0.001$), scale bar 50 µL.

Mitochondrial membrane potential disruption of A549 cells impaired by administration of EEOS

Mitochondria may be a major therapeutic target. Intrinsic apoptosis is closely related to mitochondrial disruption. Therefore, to determine the potential of EEOS against A549 cells in inducing apoptosis, mitochondrial membrane staining with JC-1 staining was performed. JC-1 staining turns mitochondria orange as a result of the formation of JC-1 aggregates, and normal cells stained with JC-1 as a monomer show green luminescence (**Figure 5(A)**). The effect of EEOS in agitating mitochondria, causing apoptosis, can be seen on the JC-1 staining. The ratio of red and green fluorescence was calculated by the ImageJ program to compare the effect of EEOS on MMP changes. As shown in **Figure 5(B)**, as the dose of EEOS increased, A549 cells showed lower red/green fluorescence, suggesting that EEOS may affect mitochondria and cause collapse in MMPs.

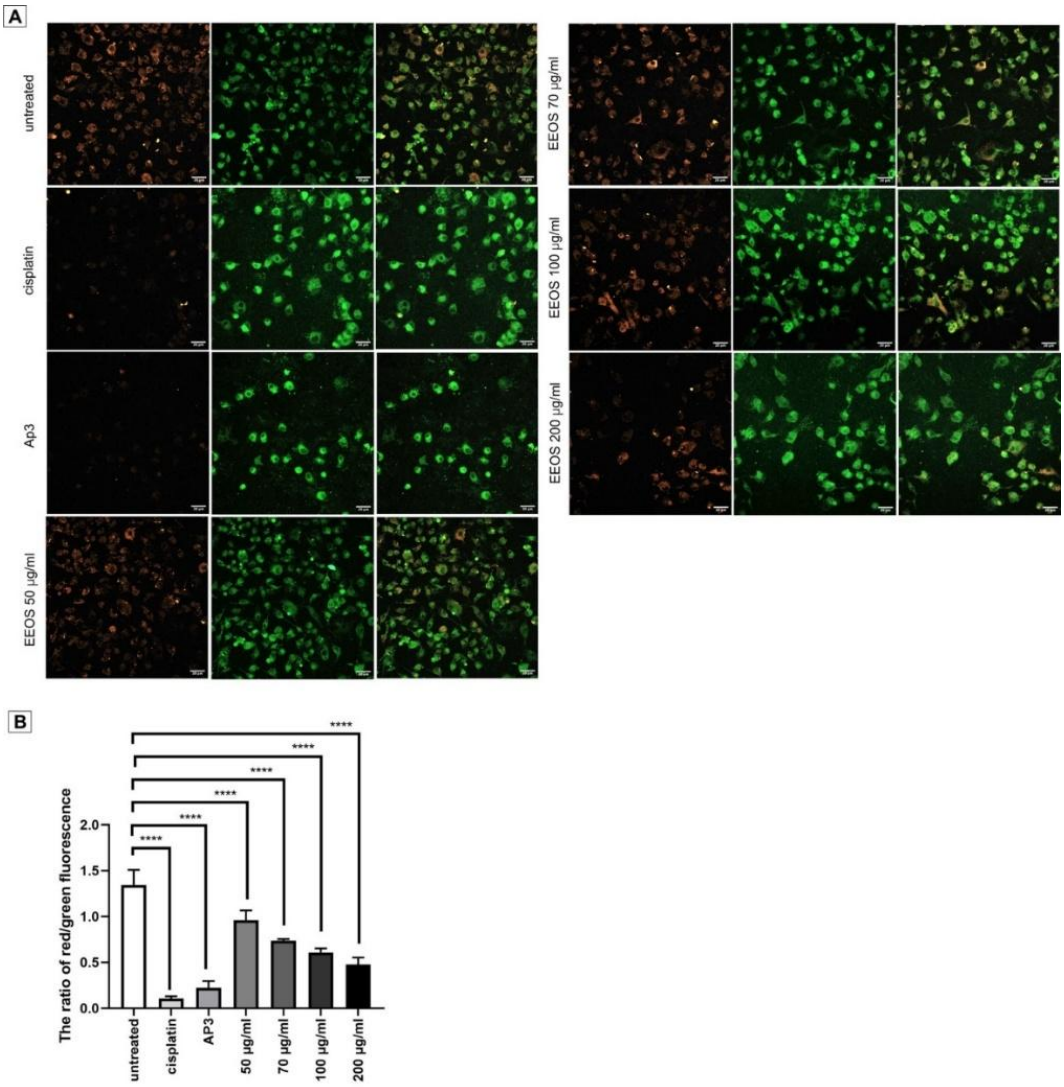

Figure 5 JC-1 Staining of A549 cells mitochondrial membrane potential assay. The depolarization of mitochondrial membrane potential cells exposed to EEOS. Polarized mitochondria accumulate more JC-1, forming red fluorescent J-aggregates, while unhealthy, depolarized mitochondria have fewer aggregates and emit more green fluorescence from JC-1 monomers. (B) Quantitative evaluation of the luminous intensity ratio between red and green was performed using a 1-way ANOVA and Tukey's post hoc; the data performed 3 replications with 3 repetition, and the results demonstrated that EEOS with a concentration of 200 µg/mL can decrease the potential membrane of mitochondria in A549 cells significantly ($p < 0.0001$). The scale bar represents 20 µm.

EEOS enhances ROS to induce apoptosis

The most important factor in eliminating cancer cells is the rise in ROS in cells. The phosphorescent DCF is formed from the oxidation of DCFH derived from esterase in DCFH-DA cells. The graph showed that in the untreated group, EEOS 50 µg/ml and EEOS 70 µg/mL were observed to be weak. A significant increase in luminescence was seen in EEOS 200 µg/mL, namely, 25.8 times compared to the control. The results showed a significant increase in ROS at EEOS 200 µg/mL, such that EEOS was able to activate apoptosis in A549 cells (**Figure 6**).

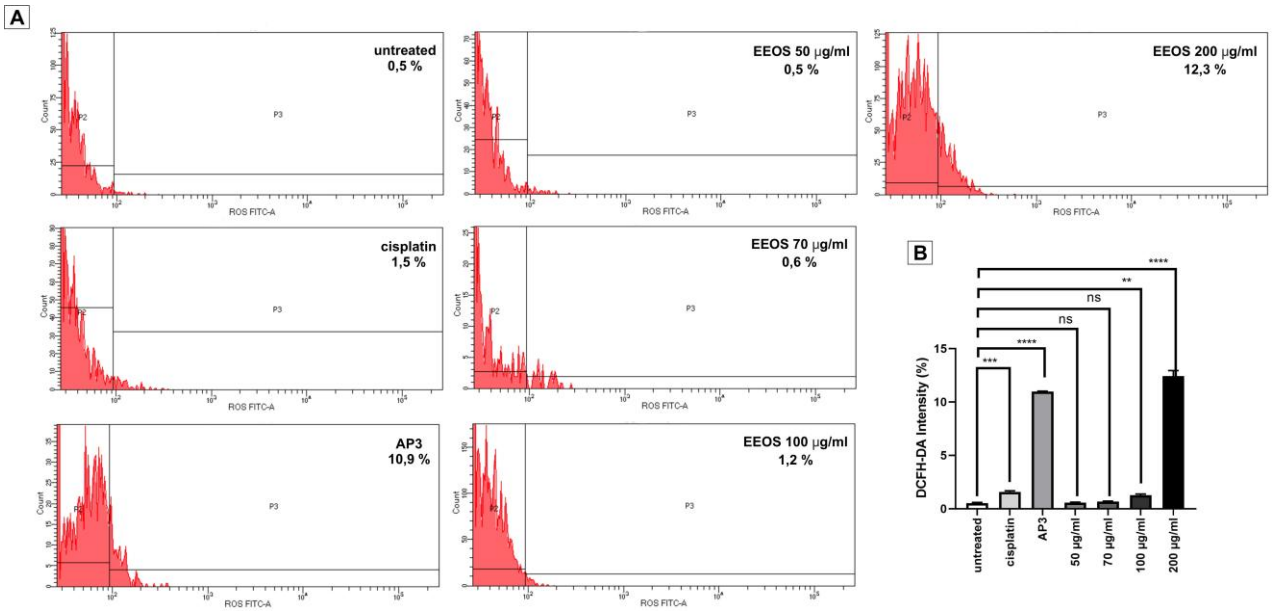

Figure 6 Flowcytometry chart of EEOS stimulating ROS to induce apoptosis in an A549 cell line. ROS levels in A549 cells treated with EEOS increased gradually and significantly in comparison to the control group. ROS was also significantly elevated in the AP3 group, which served as a positive control. The data taken in 2 replications with 3 repetitions and analyzed using a 1-way ANOVA followed by Tukey's post hoc. **) $p = 0.0098$; ***) $p = 0.0004$; ****) $p < 0.0001$; ns: non-significant.

EEOS suppresses NF-kB activity in the lung adenocarcinoma cell line A-549

To conduct a more extensive investigation of the anti-cancer efficacy of EEOS in the A-549 cell line, an enzyme-linked immunosorbent assay (ELISA) was employed to analyze the activity of NF-kB. In comparison to the untreated group, the group exposed to EEOS exhibited a significantly reduced expression level of NF-kB. Furthermore, a higher concentration of EEOS corresponded to a greater decrease in NF-kB expression ($p < 0.0001$) (**Figure 7**).

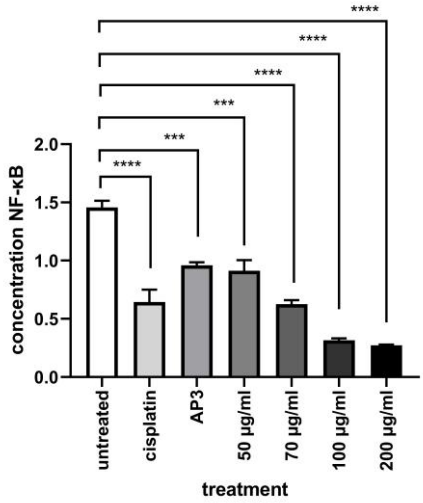

Figure 7 The ethanolic extract of *O. sanctum* Linn decreased NF-κB in A549 cells. A sandwich ELISA demonstrates decreased NF-κB expression in NSCLC (A549) (significance value $p < 0.0001$).

EEOS induced overexpression of APAF-1, Caspase-3, and Caspase-9 expression in lung adenocarcinoma cell line A-549

To enhance comprehension of the anti-cancer properties, particularly pertaining to the apoptotic mechanism of EEOS, the ELISA approach was employed to analyze the protein expression levels linked to apoptosis. The A-549 cell line was subjected to treatment with varying concentrations (50, 70, 100 and 200 µg/mL) of EEOS for a duration of 24 h. Subsequently, quantification of protein expression was carried out. After the application of EEOS therapy, there was a significant upregulation in the concentration levels of APAF-1, Caspase-9, and Caspase-3, which exhibited a dose-dependent pattern ($p < 0.001$) (**Figure 8**).

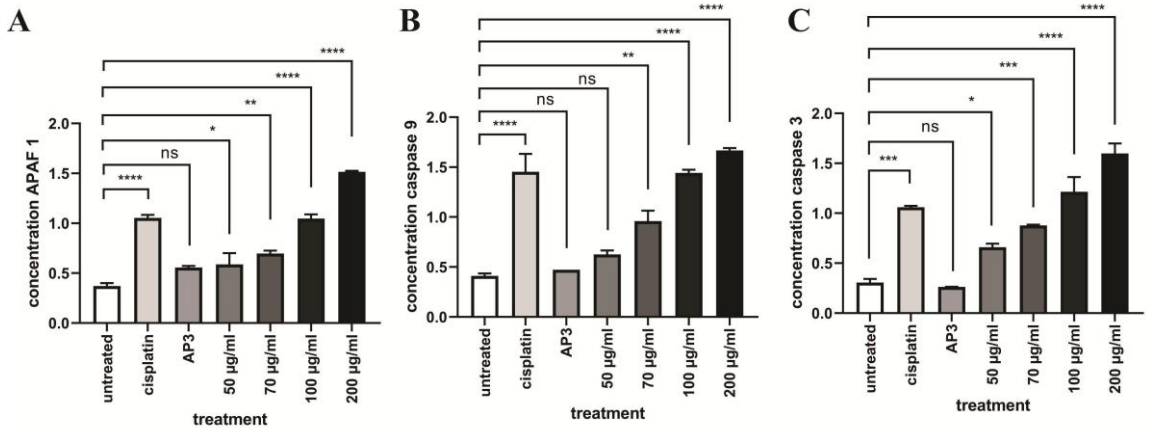

Figure 8 Ethanolic extract of *O. sanctum* Linn increases APAF-1, Caspase-9, and Caspase-3 in A549 cells. Upgraded APAF-1, Caspase-9, and Caspase-3 concentrations in NSCLC (A549) demonstrated by sandwich ELISA. (A) EEOS can significantly upgrade APAF-1, Caspase-9 significance value $p < 0.0001$, ns: non-significant.

EEOS reduced the toxic effects in mice given a single high dose of Benzo(a)pyrene in the short term.

Short-term animal models were induced in vivo using B(a)P to verify the chemopreventive efficacy of EEOS. The figure describes the experimental design. For 7 days, EEOS (150 mg/kg body weight, oral administration) was given once daily to male C3H mice. On day 7, 2 h after the medication was administered, the mice received a single oral dosage of B(a)P (125 mg/kg body weight) (**Figure 9(A)**). Lung sections subjected to histological examination (H&E) revealed that

B(a)P resulted in a significant increase in polymorphonuclear infiltration, alveolar thickness, and fibrin and elastin fibroelastosis (**Figures 9(B(b))** and **9(B(c))**, whereas the lungs of the mice treated with EEOS showed a decrease in these histopathological alterations (**Figure 9(B)**). EEOS demonstrated protective activity against acute lung tissue damage produced by B(a)P in mice given a single dosage of the drug for a limited duration. According to these findings, EEOS can reduce inflammation, DNA damage, and B(a)P-induced short-term lung toxicity - all of which have been linked to lung carcinogenesis (**Figures 9(B(e)** and **9(B(f))**. The group that only received EEOS did not show any changes indicating lung tissue damage (**Figure 9(B(d))**.

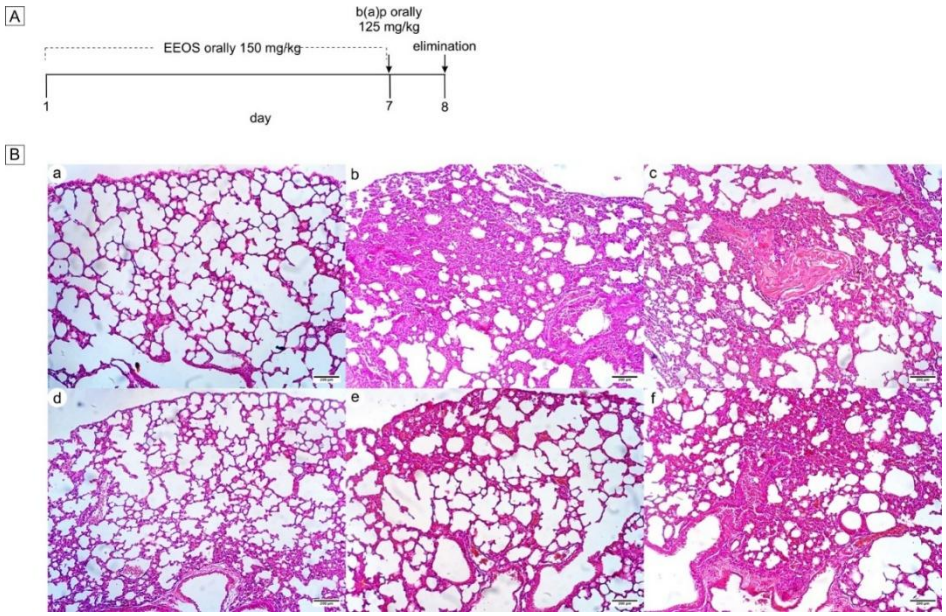

Figure 9 Effects of EEOS on a single high dose of Benzo(a)pyrene-induced lung toxicity. (A) Design of animal experiments. As a negative control, group A received corn oil as a B(a)P vehicle on day 7; as a positive control, group B received B(a)P diluted in corn oil on day 7 and as a treatment, group C received EEOS in 7 days, and group D received EEOS on 7 days and B(a)P in corn oil on day 7. (B) The impact of EEOS on B(a)P-induced histopathologic alterations: fibroelastosis and a significant polymorphonuclear infiltration were seen in the B group (b,c), whereas the C group exhibited less polymorphonuclear infiltration than the B group (e,f). Sections of the lung (×10) stained with H&E for CH_3. (a) Negative control group with corn oil, (b,c) positive control group was given B(a)P on day 7, (d) EEOS only group with 7 days' treatment, (e,f) EEOS treatment for 7 days and given B(a)p; 100 μm is the scale bar.

Secondary metabolites derived from plants are commonly implicated in treating several ailments - the present work employed GC-MS to run the metabolomic analysis on EEOS. The analysis results indicated the existence of various secondary metabolites, with linoleic acid being identified as one of the predominant constituents. Linoleic acid is a secondary metabolite derived from EEOS that exhibits various beneficial effects, including cardiovascular protection, anti-cancer properties, neuroprotection, anti-osteoporotic activity, anti-inflammatory effects, and antioxidative properties [54]. Multiple studies have demonstrated that Linoleic acid can trigger apoptosis and diminish proliferation in various cancer types, such as human melanoma cancer cell line WM793 [55] and colorectal cancer [50,56]. Linoleic acid binding with NF-κB, Apaf-1, Caspase-3, and Caspase-9 has lower affinities with energy than cisplatin as a ligand. From this finding, we can predict that linoleic acid in EEOS can inhibit NF-κB and increase the apoptosis protein to induce cell death.

O. sanctum has moderate antioxidant content. Antioxidants are substances that neutralize ROS, which are byproducts of cellular metabolism that can induce damage to cellular components, including DNA, proteins, and lipids, contributing to carcinogenesis [20,57]. In lung cancer cells, antioxidants play a dual role. They help maintain redox homeostasis and prevent oxidative stress, which is vital in protecting cells from

damage that could lead to tumorigenesis [58,59]. On the other hand, certain antioxidants can exhibit pro-oxidant behavior under specific conditions [60]. Cancer cells often have elevated levels of ROS as part of their metabolic adaptations that support rapid proliferation and invasion [61]. In these conditions, instead of neutralizing ROS, the antioxidant can induce more oxidative stress, potentially triggering apoptosis (cell death) in the cancer cells [62].

Furthermore, some studies have provided evidence of a positive correlation between the consumption of antioxidants derived from herbal sources and a range of beneficial effects on human health. Numerous diseases, including cancer, are significantly influenced by free radicals. ROS and reactive nitrogen species (RNS) are the most common types of free radicals. High accumulation of ROS and low antioxidants in cells leads to oxidative stress, which is an imbalance in redox status. ROS causes DNA strand breaks and can oxidize biological molecules such as proteins, lipids, and carbohydrates, resulting in mutagenesis and, eventually, cancer. Through both enzymatic and non-enzymatic processes, the body continuously produces free radicals. There is growing evidence that free radicals increase oxidative stress, which has a series of negative impacts on the organism [63,64]. Antioxidants are known to have an important role in minimizing the adverse effects of free radicals in various disorders, including cancer, emphasizing their considerable importance. Previous research shows that EEOS contains phenols, flavonoids, and tannins [35]. These phytochemicals are sources of antioxidant and scavenging activity. Flavonoids have antioxidant activity, will provide hydrogen molecules from hydroxyl groups, resulting in more stable and less reactive radicals, and can inhibit the initiation of oxidative reactions [65]. The current investigation provides evidence that the EEOS extract exhibits antioxidant characteristics, indicating its potential as a therapeutic intervention to ameliorate the progression of many disorders linked to oxidative stress, such as cancer. In this study, the possible antioxidant properties of inosine were investigated through GC-MS. Preceding studies have demonstrated that the ingestion of inosine through oral administration results in increased levels of antioxidants in the bloodstream [27,66].

In the current research, we inspected the cellular mechanism underlying the anti-cancer properties of EEOS. The study's findings demonstrated that the treatment of EEOS on the A549 showed suppression of the activation of NF-kB, a well-established inflammatory transcription factor playing a crucial role in several biological phenomena, and exhibited a dual impact on cancer progression. NF-κB and ROS are both key players in lung cancer development and have a reciprocal crosstalk relationship. NF-κB promotes cancer by boosting cell proliferation and survival, while ROS contributes to DNA damage and other pro-tumorigenic changes. In turn, ROS can either stimulate or inhibit NF-κB signaling, and NF-κB can regulate ROS levels, creating a complex feedback loop that drives lung tumorigenesis [67]. NF-κB is required to regulate ROS levels. In some cancers, NF-κB is activated to maintain intracellular ROS at a certain level to prevent cell death. When NF-κB is inhibited, ROS levels can increase significantly, causing activation of the proapoptotic pathway [68].

Furthermore, the research findings indicated a rise in Apaf-1 activation, along with overexpression in the expression of Caspase-9 (which serves as the initiator of apoptosis) and Caspase-3 (which acts as the executor of apoptosis), which are responsible for executing the demolition stage of apoptosis in the A549 lung cancer cell line. The trigger of apoptosis in A549 cells by EEOS can be classified as an intrinsic route. Various cellular stressors, such as DNA damage and metabolic and endoplasmic reticulum stress, predominantly initiate the activation of the intrinsic route. This pathway is activated by chemotherapeutic medications and natural treatments commonly employed in treating different types of malignancies. The stimuli, as mentioned above, converge against the mitochondria by causing the outer membrane of the mitochondria to permeate, which, in turn, releases cytochrome c from the mitochondria's intermembrane gap into the cytoplasm. Upon entering the cytoplasm, cytochrome c interacts with the WD (Tryptophan-Aspartic Acid) domain and repeats of Apaf-1, thereby triggering a conformational alteration that results in the unfolding of the molecule. Upon the presence of dATP or ATP, Apaf-1 undergoes oligomerization, leading to the assembly of the Apaf-1 apoptosome. In a sequential manner, the apoptosome attracts and initiates the activation of Caspase-9. This

activation subsequently triggers the caspase cascade by cleaving the executioner Caspase-3, as described by [69]. Our results are in accordance with prior research demonstrating the potential of natural remedies, including *Clematis flammula* L, *Oryza officinalis*, *Mylabris phelerata Pallas*, and *Tanacetum parthenium* L., to induce apoptosis in lung cancer cells [59,68,70,71]. Additionally, the efficacy of *Flemingia macrophylla* and *Camellia sinensis* on prostate cancer has been investigated [72,73]. Similarly, the impact of *Curcuma longa* and *Ulmus davidiana* var. japonica, respectively, on stomach cancer has been examined [74,75].

Finally, linoleic acid, the major compound in EEOS, exhibited strong binding affinity toward both NF-κB and Apaf-1 in silico. Binding to NF-κB likely disrupts its activation and DNA-binding capacity, suppressing the transcription of anti-apoptotic and pro-survival genes. Concurrently, linoleic acid's interaction with Apaf-1 may stabilize its active conformation, facilitating apoptosome assembly and triggering Caspase-9 and Caspase-3 activation. These computational predictions are strongly supported by our in vitro findings, where EEOS treatment suppressed NF-κB, increased Apaf-1 expression, induced mitochondrial depolarization, elevated ROS, and activated caspase-dependent apoptosis in A549 cells [76,77]. Moreover, the in vivo reduction of B[a]P-induced lung damage is consistent with NF-κB inhibition and enhanced intrinsic apoptosis, supporting the physiological relevance of these mechanisms. Together, the in silico, in vitro, and in vivo data converge to demonstrate that EEOS induces apoptosis primarily through NF-κB inhibition coupled with Apaf-1/caspase pathway activation [78].

Conclusions

The findings presented above are corroborated by the GC-MS and DPPH analysis, which verified the existence of many secondary metabolites that have been documented to have anti-cancer and antioxidant properties. Hence, it can be deduced that the observed anti-cancer properties in the ethanol extract of *O. sanctum* leaves may be attributable to the existence of these compounds. In conclusion, we have discovered previously unknown mechanisms that contribute to the apoptotic impact of the ethanol extract of *O. sanctum* on A549 lung cancer. The elements of EEOS have been found to have an inhibitory effect on the expression of NF-kB and to initiate apoptosis through the intrinsic pathway. This apoptotic process is mediated by the activation of Apaf-1, which is associated with caspases. Additional research should be conducted to extract a distinct bioactive molecule from EEOS that demonstrates efficacy in cancer treatment

Acknowledgements

We would like to express our special thanks to all staff in the Department of Pharmacology and Therapy, Faculty of Medicine, Public Health, and Nursing, University of Gadjah Mada, Indonesia for their assistance in the research. This research was funded by The Ministry of Education, Culture, Research, and Technology from Doctoral Dissertation Research Programme, grant number 2117/UN1/DITLIT/Dit-Lit/PT.01.03/2023.

Declaration of Generative AI in Scientific Writing

The authors declare that during the preparation of this manuscript, generative artificial intelligence (AI) and AI-assisted technologies were used exclusively for language refinement and editing purposes, specifically to improve grammar, syntax, clarity, and conciseness. Tools such as Grammarly and QuillBot were utilized to enhance the English language quality of the text. No generative AI tools were used for generating content, formulating arguments, analyzing data, or drawing conclusions. All content, ideas, analyses, and conclusions presented in this manuscript are solely the original work of the authors. The authors have reviewed and edited all AI-generated suggestions to ensure accuracy and scientific integrity.

CRediT Author Statement

Ulayatul Kustiati: Validation, formal analysis, investigation, writing - original draft preparation, visualization, project administration; **Dewi Ratih Tirto Sari:** Formal analysis, investigation, visualization; **Golda Rani Saragih:** validation, project administration; **Chairunisa Isnainingrum:** Formal analysis, investigation; **Muhammad Lokman Md Isa:** Visualization, validation; **Dwi Aris Agung Nugrahaningsih:** Methodology, writing - review and editing; **Yudy Tjahjono:** Data curation, writing - review and editing; **Dwi Liliek Kusindarta:** software,

validation; **Srikanth Karnati:** Conceptualization, methodology, data curation, writing - original draft preparation; **Hevi Wihadmadyatami:** Conceptualization, methodology, validation, resources, writing - original draft preparation, supervision, funding acquisition.

References

[1] KC Thandra, A Barsouk, K Saginala, JS Aluru and A Barsouk. Epidemiology of lung cancer. *Contemporary Oncology* 2021; **25(1)**, 45-52.

[2] MP Rivera, AC Mehta and MM Wahidi. Establishing the diagnosis of lung cancer: Diagnosis and management of lung cancer, 3rd ed: American College of Chest Physicians evidence-based clinical practice guidelines. *Chest* 2013; **143(5)**, e142S-e165S.

[3] SP Tarigan, NN Soeroso, CAK Tumanggor, S Gani and A Pradana. Clinical profile of male patients with non-small cell lung cancer in Adam Malik General Hospital, Medan, Indonesia. *Open Access Macedonian Journal of Medical Sciences* 2019; **7(16)**, 2612.

[4] F Bray, M Laversanne, H Sung, J Ferlay, RL Siegel, I Soerjomataram and A Jemal. Global Cancer Statistics 2022: GLOBOCAN estimates of incidence and mortality worldwide for 36 cancers in 185 countries. *CA Cancer Journal for Clinical* 2024; **74**, 229-263.

[5] Y Zhang, Y Xu, W Zhong, J Zhao, X Liu, X Gao, M Chen and M Wang. Vitamin D and immune checkpoint inhibitors in lung cancer: A synergistic approach to enhancing treatment efficacy. *International Journal of Molecular Science* 2025; **26**, 4511.

[6] Z Rahal, SE Nemr, A Sinjab, H Chami, A Tfayli and H Kadara. Smoking and lung cancer: A geo-regional perspective. *Frontiers in Oncology* 2017; **7**, 194.

[7] A Suraya, D Nowak, AW Sulistomo, AG Icksan, U Berger, E Syahruddin and S Bose-O'Reilly. Excess risk of lung cancer among agriculture and construction workers in Indonesia. *Annals of Global Health* 2021; **87(1)**, 8.

[8] X Chu, Q Wang and C Su. Indoor air pollution: An important risk factor for lung cancer among Asian women without a history of smoking. *Chinese Medical Journal Pulmonary and Critical Care Medicine* 2023; **1(04)**, 198-199.

[9] AS La'ah and SH Chiou. Cutting-edge therapies for lung cancer. *Cells* 2024; **13(5)**, 436.

[10] ZN Lei, Q Tian, QX Teng, JND Wurpel, L Zeng, Y Pan and ZS Chen. Understanding and targeting resistance mechanisms in cancer. *MedComm* 2023; **4(3)**, e265.

[11] M Greenwell and PKSM Rahman. Medicinal plants: Their use in anticancer treatment. *International Journal of Pharmaceutical Sciences and Research* 2015; **6**, 4103-4112.

[12] A Jenča, DK Mills, H Ghasemi, E Saberian, A Jenča, AMK Forood, A Petrášová, J Jenčová, ZJ Velisdeh, H Zare-Zardini and M Ebrahimifar. Herbal therapies for cancer treatment: A review of phytotherapeutic efficacy. *Biologics* 2024; **18**, 229-255.

[13] DH Tambekar and SB Dahikar. Antibacterial activity of some Indian ayurvedic preparations against enteric bacterial pathogens. *Journal of Advanced Pharmaceutical Technology and Research* 2011; **2**, 24-29.

[14] VC Pathiranage, I Thabrew, SR Samarakoon, KH Tennekoon, U Rajagopalan and MK Ediriweera. Evaluation of anticancer effects of a pharmaceutically viable extract of a traditional polyherbal mixture against non-small-cell lung cancer cells. *Journal of Integrative Medicine* 2020; **18**, 242-252.

[15] SK Jha, N Singh, OR Shanker, I Antil, JS Baghel, V Huddar and R Tripathi. A review on integrative approaches in oncology: Bridging ayurvedic medicine and modern cancer therapeutics. *Frontiers in Natural Product* 2025; **4**, 1635197.

[16] L Rombolà, D Scuteri, S Marilisa, C Watanabe, LA Morrone, G Bagetta and MT Corasaniti. Pharmacokinetic interactions between herbal medicines and drugs: Their mechanisms and clinical relevance. *Life* 2020; **10(7)**, 106.

[17] A Okem, C Henstra, M Lambert and R Hayeshi. A review of the pharmacodynamic effect of chemo-herbal drug combinations therapy for cancer treatment. *Medical in Drug Discovery* 2023; **17**, 100147.

[18] D Cui, C Zhang, L Zhang, J Zheng, J Wang, L He, H Jin, Q Kang, Y Zhang, N Li, Z Sun, W Zheng, J Wei, S Zhang, Y Bin, W Tan and Z Zhong. Natural anti-cancer products: Insights from herbal medicine. *Chinese Medicine* 2025; **20**, 82.

[19] S Zamani, M Fathi, MT Ebadi and A Mathe. Global trade of medical and aromatic plants: A review. *Journal of Agruculture and Food Research* 2025; **21**, 101910.

[20] K Utispan, N Niyomtham, BE Yingyongnarongkul and S Koontongkaew. Ethanolic extract of Ocimum sanctum leaves reduced invasion and matrix metalloproteinase activity of head and neck cancer cell lines. *Asian Pacific Journal of Cancer Prevention* 2020; **21**, 363-370.

[21] MM Cohen. Tulsi - Ocimum sanctum: A herb for all reasons. *Journal of Ayurveda and Integrative Medicine* 2014; **5**, 251-259.

[22] K Jaye, IH Dissanayake, DJ Bhuyan and D Chang. A scoping review of chemical, pharmacological and toxicological properties and clinical applications of Australian indigenous medicine. *Biomedicine & Pharmacotherapy* 2025; **191**, 118503.

[23] D Pradhan, P Biswasroy, J Haldar, P Cheruvanachari, D Dubey, VK Rai, B Kar, DM Kar, G Rath and G Ghosh. A comprehensive review on phytochemistry, molecular pharmacology, clinical and translational outfit of *Ocimum sanctum* L. *South African Journal of Botany* 2022; **150**, 342-360.

[24] DL Kusindarta, H Wihadmadyatami and A Haryanto. The analysis of hippocampus neuronal density (CA1 and CA3) after Ocimum sanctum ethanolic extract treatment on the young adulthood and middle-aged rat model. *Veterinary World* 2018; **11(2)**, 135-140.

[25] T Manaharan, R Thirugnanasampandan, R Jayakumar, G Ramya, G Ramnath and MS Kanthimathi. Antimetastatic and anti-inflammatory potentials of essential oil from edible ocimum sanctum leaves. *Scientific World Journal* 2014; **2014**, 239508.

[26] P Eswar, CG Devaraj and P Agarwal. Anti-microbial activity of tulsi {*Ocimum Sanctum* (Linn)} extract on a periodontal pathogen in human dental plaque: An invitro study. *Journal of Clinical and Diagnostic Research* 2016; **10(3)**, 53-56.

[27] S Bhattacharyya, R Bakshi, R Logan, A Ascherio, EA Macklin and MA Schwarzschild. Oral inosine persistently elevates plasma antioxidant capacity in Parkinson's disease. *Movement Disorders* 2016; **31(3)**, 417-421.

[28] P Manikandan, RS Murugan, H Abbas, SK Abraham and S Nagini. *Ocimum sanctum* Linn. (Holy Basil) ethanolic leaf extract protects against 7,12-dimethylbenz[a]anthracene-induced genotoxicity, oxidative stress, and imbalance in xenobiotic-metabolizing enzymes. *Journal of Medicinal Food* 2007; **10(3)**, 495-502.

[29] T Shimizu, MP Torres, S Chakraborty, JJ Souchek, S Rachagani, S Kaur, M Macha, AK Ganti, RJ Hauke and SK Batra. Holy basil leaf extract decreases tumorigenicity and metastasis of aggressive human pancreatic cancer cells *in vitro* and in vivo: Potential role in therapy. *Cancer letters* 2013; **336(2)**, 270-280.

[30] MR Hasan, BS Alotaibi, ZM Althafar, AH Mujamammi and J Jameela. An update on the therapeutic anticancer potential of *Ocimum sanctum* L.: "Elixir of Life.". *Molecules* 2023; **28(3)**, 1193.

[31] U Kustiati, S Ergün, S Karnati, DAA Nugrahaningsih, DL Kusindarta and H Wihadmadyatami. Ethanolic extract of *Ocimum sanctum* Linn. inhibits cell migration of human lung adenocarcinoma cells (A549) by downregulation of integrin αvβ3, α5β1, and VEGF. *Scientia Pharmaceutica* 2022; **90(4)**, 69.

[32] AM Luke, R Patnaik, ST Kuriadom, M Jaber and S Mathew. An *in vitro* study of *Ocimum sanctum* as a chemotherapeutic agent on oral cancer cell-line. *Saudi Journal of Biological Sciences* 2021; **28(1)**, 887-890.

[33] RR Rasmi, KM Sakthivel and C Guruvayoorappan. NF-κB inhibitors in treatment and prevention of lung cancer. *Biomedicine & Pharmacotherapy* 2020; **130**, 110569.

[34] H Wihadmadyatami, S Karnati, P Hening, Y Tjahjono, Rizal, F Maharjanti F, DL Kusindarta, T Triyono and Supriyanto. Ethanolic extract

Ocimum sanctum Linn. induces an apoptosis in human lung adenocarcinoma (A549) cells. *Heliyon* 2019; **5(11)**, e020772.

[35] U Kustiati, H Wihadmadyatami and DL Kusindarta. Dataset of phytochemical and secondary metabolite profiling of holy basil leaf (*Ocimum sanctum* Linn) ethanolic extract using spectrophotometry, thin layer chromatography, Fourier transform infrared spectroscopy, and nuclear magnetic resonance. *Data in Brief* 2021; **40**, 107774

[36] LA Putri, I Rahman, M Puspita, SN Hidayat, AB Dharmawan, A Rianjanu, S Wibirama, R Roto, K Triyana and HS Wasisto. Rapid analysis of meat floss origin using a supervised machine learning-based electronic nose towards food authentication. *NPJ Science of Food* 2023; **7(1)**, 31.

[37] J Sukweenadhi, O Yunita, F Setiawan, Kartini, MT Siagian, AP Danduru and C Avanti. Antioxidant activity screening of 7 Indonesian herbal extract. *Biodiversitas* 2020; **21(5)**, 2062-2067.

[38] T Furuhashi and K Okuda. Application of GC/MS soft ionization for isomeric biological compound analysis. *Critical Reviews in Analytical Chemistry* 2017; **47(5)**, 438-453.

[39] NA Byrnes, Y Wu, Y Nolvachai and PJ Marriott. Exploring thermal isomerisation in gas chromatography analyses using natural pyrethrins: Comparison of comprehensive two-dimensional and one-dimensional gas chromatography. *Journal of Chromatography A*2023; **1708**, 464369.

[40] D Cyr, M Boutin, B Maranda and PJ Waters. Enhanced differentiation between 3-hydroxyglutaric and 2-hydroxyglutaric acids facilitates diagnostic testing for glutaric aciduria type 1. *JIMD Reports* 2024; **65**, 433-441.

[41] M Zbiljić, J Šinžar-Sekulić, D Lakušić, D Stojanović, B Lakušić and M Marčetić. *Teucrium montanum* essential oils variability in the Balkan Peninsula. *Chemistry & Biodiversity* 2025; **22(10)**, e00561.

[42] X Fu, Z Xu, M Gawaz and M Lämmerhofer. UHPLC-MS/MS method for chiral separation of 3-hydroxy fatty acids on amylose-based chiral stationary phase and its application for the enantioselective analysis in plasma and platelets. *Journal of Pharmaceutical and Biomedical Analysis* 2023; **223**, 115151.

[43] K Singh, M Bhori, YA Kasu, G Bhat and T Marar. Antioxidants as precision weapons in war against cancer chemotherapy induced toxicity - exploring the armoury of obscurity. *Saudi Pharmaceutical Journal* 2018; **26(2)**, 177-190.

[44] AS Choudhari, PC Mandave, M Deshpande, P Ranjekar and O Prakash. Phytochemicals in cancer treatment: From preclinical studies to clinical practice. *Frontiers in Pharmacology* 2020; **10**, 1614.

[45] T Siddiqui, MU Khan, V Sharma and K Gupta. Terpenoids in essential oils: Chemistry, classification, and potential impact on human health and industry. *Phytomedicine Plus* 2024; **4(2)**, 100549.

[46] Y Dong, Z Wei, W Zhang, J Li, M Han, H Bai, H Bai, H Li and L Shi. LaMYC7, a positive regulator of linalool and caryophyllene biosynthesis, confers plant resistance to *Pseudomonas syringae*. *Horticulture Research* 2024; **11(4)**, uhae044.

[47] T Abu-Izneid, A Rauf, MA Shariati, AA Khalil, M Imran, M Rebezov, MS Uddin, MF Mahomoodally and KRR Rengasamy. Sesquiterpenes and their derivatives-natural anticancer compounds: An update. *Pharmacological Research* 2020; **161**, 105165.

[48] N Arizmendi, SB Alam, K Azyat, D Makeiff, AD Befus and M Kulka. The complexity of sesquiterpene chemistry dictates its pleiotropic biologic effects on inflammation. *Molecules* 2022; **27(8)**, 2450.

[49] CMC Andrés, EB Munguira, CA Juan, F Lobo, E Pérez-Lebeña and JMP de la Lastra. *In silico* exploration of natural antioxidants for sepsis drug discovery. *Molecules* 2025; **30(11)**, 2288.

[50] J Mercola. Historical rise of cancer and dietary linoleic acid: Mechanisms and therapeutic strategies. *World Journal of Clinical Oncology* 2025; **16(9)**, 110686.

[51] G Mustafa, S Younas, H Mahrosh, M Albeshr and E Bhat. Molecular docking and simulation-binding analysis of plant phytochemicals with the hepatocellular carcinoma targets epidermal

growth factor receptor and caspase-9. *Molecules* 2023; **28(8)**, 3583.

[52] M Shamsuzzaman, K Kalaiselvi and M Prabakaran. Evaluation of antioxidant and anticorrosive activities of ceriops tagal plant extract. *Applied Sciences* 2021, **11(21)**, 10150.

[53] S Phongpaichit, J Nikom, N Rungjindamai, J Sakayaroj, N Hutadilok-Towatana, V Rukachaisirikul and K Kirtikara. Biological activities of extracts from endophytic fungi isolated from Garcinia plants. *FEMS Immunology and Medical Microbiology* 2007; **51(3)**, 517-525.

[54] KB Kim, YA Nam, HS Kim, AW Hayes and BM Lee. α-Linolenic acid: Nutraceutical, pharmacological and toxicological evaluation. *Food and Chemical Toxicology* 2014; **70**, 163-178.

[55] D Domagala, T Leszczynska, A Koronowicz, B Domagala, M Drozdowska and E Piasna-alupecka. Mechanisms of anticancer activity of a fatty acid mixture extracted from hen egg yolks enriched in conjugated linoleic acid diene (Cla) against wm793 melanoma cells. *Nutrients* 2021; **13(7)**, 2348.

[56] X Lu, H Yu, Q Ma, S Shen and UN Das. Linoleic acid suppresses colorectal cancer cell growth by inducing oxidant stress and mitochondrial dysfunction. *Lipids in Health and Disease* 2010; **9**, 106.

[57] A Chaudhary, S Sharma, A Mittal, S Gupta and A Dua. Phytochemical and antioxidant profiling of *Ocimum sanctum*. *Journal of food science and technology* 2020; **57(10)**, 3852-3863.

[58] RM Sáinz, RJ Reiter, D Ta, F Roldan, M Natarajan I Quirós-González, D Hevia, C Rodriguez and JC Mayo. Critical role of glutathione in melatonin enhancement of tumor necrosis factor and ionizing radiation-induced apoptosis in prostate cancer cells *in vitro*. *Journal of pineal research* 2008; **45(3)**, 258-270.

[59] KM Yang, BM Kim and JB Park. ω-Hydroxyundec-9-enoic acid induces apoptosis through ROS-mediated endoplasmic reticulum stress in non-small cell lung cancer cells. *Biochemical and Biophysical Research Communications* 2014; **448(3)**, 267-273.

[60] Y Liu, G Wu, L Feng, J Li, Y Xia, W Guo and K Zhao. Harnessing antioxidants in cancer therapy: Opportunities, challenges, and future directions. *Antioxidants* 2025; **14(6)**, 674.

[61] W Deng, Y Zhang, J Cai, J Zhang, X Liu, J Yin, Z Bai, H Yao and Z Zhang. LncRNA-ANRIL promotes gastric cancer progression by enhancing NF-kB signaling. *Experimental Biology and Medicine* 2019; **244(12)**, 953-959.

[62] J Shin, MH Song, JW Oh, YS Keum and RK Saini. Pro-oxidant actions of carotenoids in triggering apoptosis of cancer cells: A review of emerging evidence. *Antioxidants* 2020; **9(6)**, 532.

[63] DP Xu, Y Li, X Meng, T Zhou, Y Zhou, J Zheng, JJ Zhang and HB Li. Natural antioxidants in foods and medicinal plants: Extraction, assessment and resources. *International Journal of Molecular Sciences* 2017; **18(1)**, 96.

[64] N Gupta, K Verma, S Nalla, A Kulshreshtha, R Lall and S Prasad. Free radicals as a double-edged sword: The cancer preventive and therapeutic roles of curcumin. *Molecules* 2020; **25(22)**, 5390.

[65] CA Juan, JMP de la Lastra, FJ Plou and E Pérez-Lebeña. The chemistry of Reactive Oxygen Species (ROS) revisited: Outlining their role in biological macromolecules (DNA, lipids and proteins) and induced pathologies. *International Journal of Molecular Sciences* 2021; **22(9)**, 4642.

[66] LP Bonagurio, AE Murakami, CA Moreira, JF Comar and PC Pozza. Dietary supplementation with inosine-5′-monophosphate improves the functional, energetic, and antioxidant status of liver and muscle growth in pigs. *Scientific Reports* 2022; **12(1)**, 350.

[67] C Guan, X Zhou, H Li, X Ma and J Zhuang. NF-κB inhibitors gifted by nature: The anticancer promise of polyphenol compounds. *Biomedicine & Pharmacotherapy* 2022; **156**,113951.

[68] MS Basile, P Bramanti and E Mazzon. Inosine in neurodegenerative diseases: From the bench to the bedside. *Molecules* 2022; **27(14)**, 4644.

[69] A Boice and L Bouchier-Hayes. Targeting apoptotic caspases in cancer. *Biochimica et biophysica acta*. *Molecular Cell Research* 2020; **1867(6)**, 118688.

[70] TC Hsia, CC Yu, SC Hsu, NY Tang, HF Lu, YP Huang, SH Wu, JG Lin and JG Chung.

Cantharidin induces apoptosis of H460 human lung cancer cells through mitochondria-dependent pathways. *International Journal of Oncology* 2014; **45(1)**, 245-254.

[71] LL Pan, XL Wang, QY Zhang, XL Luo, P Xu, SY Liu, JF Hu and XH Liu. Boehmenan, a lignan from the Chinese medicinal plant *Clematis armandii*, induces apoptosis in lung cancer cells through modulation of EGF-dependent pathways. *Phytomedicine* 2016; **23(5)**, 468-476.

[72] HD Cho, JH Lee, KD Moon, KH Park, MH Lee and KI Se. Auriculasin-induced ROS causes prostate cancer cell death via induction of apoptosis. *Food and Chemical Toxicology* 2018; **111**, 660-669.

[73] F Rizzi, V Naponelli, A Silva, A Modernelli, I Ramazzina, M Bonacini, S Tardito, R Gatti, J Uggeri and S Bettuzzi. Polyphenon E(R), a standardized green tea extract, induces endoplasmic reticulum stress, leading to death of immortalized PNT1a cells by anoikis and tumorigenic PC3 by necroptosis. *Carcinogenesis* 2014; **35(4)**, 828-839.

[74] A Cao, Q Li, P Yin, Y Dong, H Shi, Wang, G Ji, J Xie and D Wu. Curcumin induces apoptosis in human gastric carcinoma AGS cells and colon carcinoma HT-29 cells through mitochondrial dysfunction and endoplasmic reticulum stress. *Apoptosis* 2013; **18(11)**, 1391-1402.

[75] J Ahn, JS Lee and KM Yang. Ultrafine particles of Ulmus davidiana var. Japonica induce apoptosis of gastric cancer cells via activation of caspase and endoplasmic reticulum stress. *Archives of Pharmacal Research* 2014; **37(6)**, 783-792.

[76] U Kustiati, DRT Sari, DAA Nugrahaningsih, DL Kusindarta and H Wihadmadyatami. *In silico* molecular docking and in vitro analysis of ethanolic extract ocimum sanctum linn.: Inhibitory and apoptotic effects against non-small cell lung cancer. *Veterinary World* 2014; **14(12**), 3175-3187.

[77] W Wang, J Guan, Y Feng, L Nie, Y Xu, H Xu and F Fu. Polystyrene microplastics induced nephrotoxicity associated with oxidative stress, inflammation, and endoplasmic reticulum stress in juvenile rats. *Frontiers in Nutrition* 2023; **9**, 1059660.

[78] BD Wagle, AV Deshmukh, SN Mangam and NM Gangane. Can Caspase-3 act as a potential prognostic biomarker in breast cancer? - A retrospective pilot study in central India. *International Journal of Clinical and Diagnostic* 2023; **6(2)**, 76-83.